ACS APPLIED MATERIALS & INTERFACES

Research Article

www.acsami.org

Molecular Interdiffusion between Stacked Layers by Solution and Thermal Annealing Processes in Organic Light Emitting Devices

Satoru Ohisa,[†] Yong-Jin Pu,[*,†] Norifumi L. Yamada,[‡] Go Matsuba,[§] and Junji Kido[*,†]

[†]Department of Organic Device Engineering, Yamagata University, 4-3-16 Johnan, Yonezawa, Yamagata 992-8510, Japan

[‡]Institute of Material Structure Science, High-Energy Accelerator Research Organization (KEK), 203-1 Shirakata, Tokai, Naka 319-1106, Japan

[§]Department of Polymer Science and Engineering, Yamagata University, 4-3-16 Jonan, Yonezawa, Yamagata 992-8510, Japan

Supporting Information

ABSTRACT: In organic light emitting devices (OLEDs), interfacial structures between multilayers have large impacts on the characteristics of OLEDs. Herein, we succeeded in revealing the interdiffusion in solution processed and thermal annealed OLEDs by neutron reflectometry. We investigated interfaces between a polymer under layer and small molecules upper layer. The small molecules diffused into the swollen polymer layer during the interfacial formation by the solution process, but the polymer did not diffuse into the small molecules layer. At temperatures close to the glass transition temperatures of the materials, asymmetric molecular diffusion was observed. We elucidated the effects of the interdiffusion on the characteristics of OLEDs. Partially mixing the interface improved the current efficiencies due to suppressed triplet-polaron quenching at the interface. Controlling and understanding the interfacial structures of the miultilayers will be more important to improve the OLED characteristics.

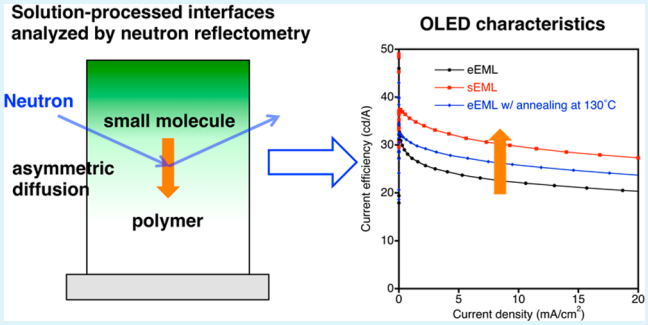

KEYWORDS: *neutron reflectometry, interface, asymmetric diffusion, thermal diffusion, charge accumulation, poly-TPD*

1. INTRODUCTION

Layered stacks of materials are a key technology for realizing various functionalities such as high-reflectivity dielectric multilayer mirrors, heat-ray cut filters, manifestation of structural colors, and films that serve as barriers to moisture and oxygen.[1−4] In general, organic optoelectronic devices, such as organic light-emitting devices (OLEDs), organic field-effect transistors, and organic photovoltaics (OPVs), have multilayer structures in which each layer has a thickness of several tens of nanometers. In such structures, different functionalities are separated into different functional materials (charge injection, charge transport, light emission, etc.). To ensure proper performances of the devices, clear interfaces are required between the layers.

These multilayer structures should be stable under external stimulations such as thermal stress and device operation. However, unfortunately, it is known that these multilayer structures can be easily disturbed under thermal stress. Smith et al. have reported on thermal diffusion in multilayer films of small molecules in dry-processed OLEDs.[5] They showed that interdiffusion between the layers can rapidly occur under high temperature environments, for example car cabins in which the devices could be located.

Recently, solution-processed organic and organic−inorganic hybrid light-emitting devices have been developed to lower production costs of the devices.[6−11] In the solution-process, in addition to the diffusion under the thermal stress, interdiffusion between multilayers can occur during formation of an interface from solution. To form a multilayer film by the solution process, the solvent used in the formation of an upper layer should not dissolve an under layer. However, differences between interfacial structures in the multilayers formed by solution and evaporation processes, have not been understood, although the interfacial structures significantly affect device performances. Further, in the solution-process, drying is inevitably necessary, and thermal annealing, far more than drying, is usually preferable to improve the quality of the films. This thermal annealing can also disturb the multilayer structure.

There have been several reports on interfacial analyses of organic optoelectronic devices by neutron reflectometry (NR).[5,6,12−18] NR is nondestructive method and has angstrom-ordered resolution along depth direction, enabling quantitative evaluation of the composition of organic/organic interface.[19−21] Refractive index contrasts between adjacent layers can be made by deuteration of the compounds. Deuteration has minimal impact on the thermodynamics of

Received: June 29, 2015
Accepted: September 2, 2015
Published: September 2, 2015

DOI: 10.1021/acsami.5b05818
ACS Appl. Mater. Interfaces 2015, 7, 20779−20785

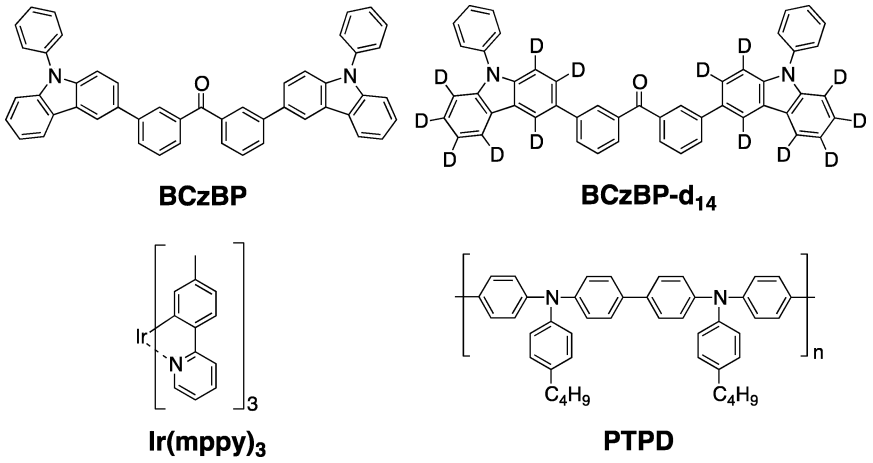

Figure 1. Chemical compounds used in evaluations of interfacial structure.

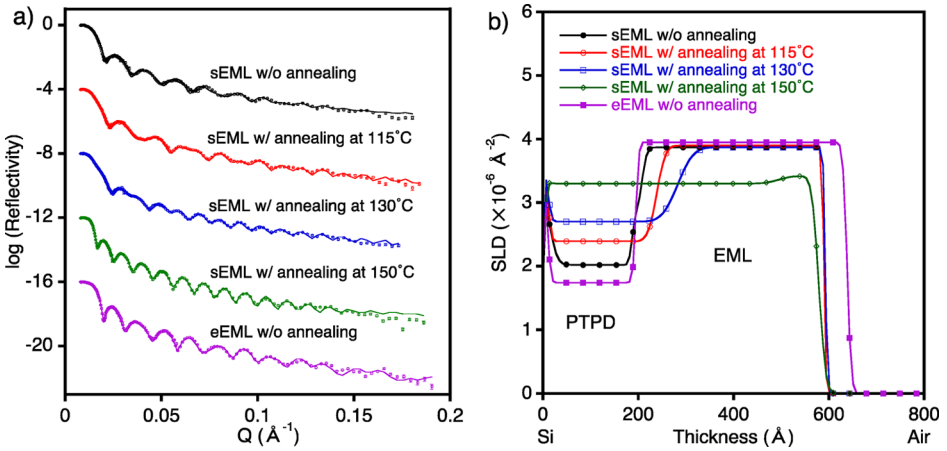

Figure 2. Neutron reflectometry results of PTPD/EML. (a) Reflectivity profiles and (b) scattering density profiles: (●) Si/PTPD/sEML without annealing; Si/PTPD/sEML with annealing at (○) 115, (□) 130, and (◊) 150 °C; and (■) Si/PTPD/eEML without annealing. The reflectivity scale corresponds to the profile for Si/PTPD/sEML without annealing. For clarity, the other plots are successively offset by subtracting 4. The reflectivity curfve of Si/PTPD/sEML without annealing was fitted with a three-layer model, and the others were fitted with two-layer models. eEML, evaporated BCzBP-d_{14}:9 wt % Ir(mppy)$_3$, and sEML, spin-coated BCzBP-d_{14}:9 wt % Ir(mppy)$_3$.

organic systems such as the interfacial formation. X-ray techniques also have angstrom-ordered resolution; however, it is difficult to enhance the contrast between adjacent layers of the organic compounds in the devices. In NR analysis, scattering length densities (SLDs) profiles are modeled, and the modeled profiles are used to calculate reflectivity curves, fitting to a measured reflectivity curve. Material compositions in each layer can be calculated from the SLD values. In the several reports, especially, interfaces between poly(3-hexylthiophene-2,5-diyl) (P3HT) and [6,6]-phenyl-C61-butyric acid methyl ester (PCBM) in OPVs have been well investigated.[12,14−16] Effects of the revealed interfacial structures on the device characteristics have been discussed. In contrast, although there have been several reports on the interfacial analyses in OLEDs, in fact, the effects of the interfacial structures on the device characteristics have almost not been discussed.[5,17,18] Especially, to our best of knowledge, there have been no detailed reports of how solution- and thermal-annealed interfaces affect the OLED characteristics, despite of the intrinsic importance. The interfacial structures can largely affect the charge injection, charge transport, and charge and exciton confinements.

Here, we report on analyses of the interface between a polymer hole transport layer and small-molecule phosphorescent emitting layer, formed by the solution process and interdiffusion between the layers by thermal annealing process, with NR and fluorescence resonance energy transfer (FRET) measurement. Further, we investigated the effects of molecular diffusions on the characteristics of OLEDs fabricated by the solution process. The compounds used in this work are shown in Figure 1. Poly[*N*,*N*′-bis(4-butylphenyl)-*N*,*N*′-bis(phenyl)-benzidine] (PTPD) was used as a hole-transporting layer. Tris(2-(4-methylphenyl)pyridine)iridium(III) (Ir(mppy)$_3$) was used as an emitter in the emitting layer. 3,3′-[Bis(9,9′-phenylcarbazol-3-yl)]-benzophenone (BCzBP) (or deuterated BCzBP (BCzBP-d_{14}) to enhance contrast) was used as host materials in the emitting layer. One component in the emitting layer was selectively deuterated. Here, PTPD has a much higher glass transition temperature (T_g; 224 °C) than those of BCzBP (119 °C) and BCzBP-d_{14} (120 °C). Preparation and characteristics evaluations of the materials were described in Supporting Information (Figures S1−S6 and Table S1). The solution-processed and evaporated emitting layer are abbreviated by sEML and eEML, respectively.

DOI: 10.1021/acsami.5b05818
ACS Appl. Mater. Interfaces 2015, 7, 20779−20785

2. RESULTS AND DISCUSSION

Prior to the investigation of the two-layer stacked films, single layer films were evaluated, because the two-layer stacked films are analyzed based on the results of the single layer films. Details of all NR results are described in the Supporting Information (Figure S7 and Table S2). In the fabrication of the two-layer stacked films, PTPD was spin coated onto a Si wafer and annealed at 135 °C for 10 min, and then BCzBP-d_{14}:9 wt % Ir(mppy)$_3$ (sEML) was spin coated onto the PTPD film. The spin coating conditions of the PTPD and sEML solutions were the same as those used to form the single layer films. BCzBP-d_{14}:9 wt % Ir(mppy)$_3$ was also coevaporated (eEML) onto a PTPD film under vacuum to form [PTPD/eEML] for comparison with [PTPD/sEML]. The fabricated [PTPD/sEML] and [PTPD/eEML] films were not annealed. NR of these films were performed (Figure 2 and Table S2). The reflectivity curve for the [PTPD/eEML] film was well represented by a two-organic-layer model. Thicknesses and SLDs of PTPD and eEML in [PTPD/eEML] were the same as those for the PTPD and eEML single-layer films, respectively. The results indicate that the interface of [PTPD/eEML] was relatively sharp and showed the interfacial roughness of 5 Å, which indicate PTPD and eEML did not diffuse each other. The reflectivity curve for [PTPD/sEML] was able to be fit to a three-organic-layer model comprising two PTPD layers and one sEML (Figure S8 and Table S3). The SLD of PTPD in [PTPD/sEML] was larger than that of the single layer film, while the SLD of sEML in [PTPD/sEML] was similar to that of the sEML single-layer film. This indicates that only sEML molecules diffused into the PTPD layer. A volume ratio of sEML molecules in the diffused PTPD layer can be calculated to be 13% from the SLD values. In our previous work, we spin-coated small molecules on a cross-linked polymer layer, and the stacked films were not thermal annealed.[6] Although the cross-linked polymer was not dissolved in the upper layer coating solvents, we observed that the small molecules diffused into the polymer layer. The polymer was swollen by the solvents, and the small molecules diffused into spaces generated by swelling. The formed interfaces were well expressed by two-layer models. In this study, PTPD was not cross-linked and slightly dissolved in the sEML coating solvent (Figure S9). The reason the [PTPD/sEML without annealing] film was not expressed by the two-layer model is probably related to the slight dissolution. PTPD was swollen by the upper coating solvent, and then the sEML molecules diffused into the spaces generated by swelling. There are solvent uptakes into the layers. However, the quantities were very low, because the layer thicknesses was almost not changed by thermal annealing described below. The slight solvent uptakes could not affect the SLD values in effect.

We also evaluated the thermal stability of the stacked films. [PTPD/sEML] was fabricated according to the same procedure, and thermal annealed at 115, 130, or 150 °C for 10 min. The thickness and SLD of PTPD in [PTPD/annealed-sEML] increased as the annealing temperature increased, compared to those of PTPD in [PTPD/sEML without thermal annealing]. Thicknesses of sEML in [PTPD/annealed-sEML] decreased as the annealing temperature increased, compared to that of sEML in [PTPD/sEML without thermal annealing]. The SLDs of sEML in [PTPD/sEML] annealed at 115 and 130 °C were almost the same as that of sEML in [PTPD/sEML without thermal annealing]. These results demonstrate asymmetric diffusion due to the much larger diffusivity of sEML molecules than that of the polymer, PTPD. We were not able to observe the SLD gradient in PTPD, probably because the diffusion time of sEML into PTPD is too short due to the thin PTPD layer (18.5 nm). In contrast, the increase in the SLD of the PTPD layer is ascribed to the increase in the amount of diffused sEML in the PTPD layer. There is a thermodynamic explanation for the asymmetric diffusion instead of the above kinetic explanation. When one material mixes with another material, the thermally equilibrated miscible system is most stable at a particular mixing ratio. In this study, when the PTPD/EML stacked films were annealed at some temperatures, the mixed layer comprising of PTPD and EML molecules can be thermally most stable at particular mixing ratios, resulting in the asymmetric diffusion. The thermal equilibration of the layer at specific mixed ratios is also consistent to the fact that no material constituent gradient was observed. After annealing at 150 °C, the stacked film was almost mixed, leaving 84 Å of less mixed sEML. The two-layer model certainly better fitted than single layer model representing completely mixing. However, the fitting difference among the both models is small, it is difficult to have a clear notion of a surface segregation indicated by the two-layer model. In the films annealed at 115, 130, and 150 °C, calculated volume ratios of sEML molecules in the diffused PTPD layers were 30, 44, and 72%, respectively. The value of 72% is consistent to a ratio of sEML single layer film thickness (69%) in the total thickness of the stacked film. This supported that the quantitative analysis of material composition by NR were reliable. Thermal diffusion occurred at temperatures much lower than the T_g of the polymer, 224 °C for PTPD, measured with differential scanning calorimetry (DSC). The annealing temperatures of 130 and 150 °C are higher than the T_g of BCzBP-d_{14}, 120 °C, and at those temperatures, sEML was in liquid state. Thus, we considered that sEML as a solvent dissolved PTPD. We assume that the small molecules diffused into the PTPD layer with unraveling the dense chains of PTPD. When the polymer chains of PTPD dissolved into the sEML layer as a solvent, the sEML molecules also diffused into the generated empty spaces of PTPD layer at the same time. The thermal diffusion of sEML into PTPD also occurred at temperature even lower than T_g of BCzBP-d_{14}. This is presumably because the T_g of BCzBP-d_{14} film is slightly different from that of bulk BCzBP-d_{14} measured by DSC.[22−25] It is noteworthy that the observed results in this work opposed previously reported results. Smith et al. reported that interdiffusions between trilayers with a structure of [deuterated bathocuproine (d-BCP)/4,4′-bis(*N*-carbazolyl)-1,1′-biphenyl (CBP) doped with tris(2-phenylpyridinato)iridium(III) (Ir(ppy)$_3$)/deuterated tris(4-carbazoyl-9-ylphenyl)amine (d-TCTA)].[6] The trilayer films were annealed at 100 °C. Interdiffusions between d-BCP and CBP:Ir(ppy)$_3$ were observed. On the other hand, interdiffusions between CBP:Ir(ppy)$_3$ and d-TCTA were not observed. Here, the annealing temperature of 100 °C was over the T_g values of BCP and CBP, but much lower than the T_g of TCTA. However, in this work, the interdiffusions between PTPD and EML were observed at the temperature much less than the T_g of PTPD. There is a possibility that the diffusion behavior relates with materials miscibility and film morphology.

The diffusion of EML molecules into the PTPD layer was also investigated using FRET measurements. Stacked films with the structure of [quartz/PTPD (20 nm)/BCzBP:9 wt % Ir(mppy)$_3$ (40 nm)] were fabricated. BCzBP:9 wt % Ir(mppy)$_3$

DOI: 10.1021/acsami.5b05818
ACS Appl. Mater. Interfaces 2015, 7, 20779−20785

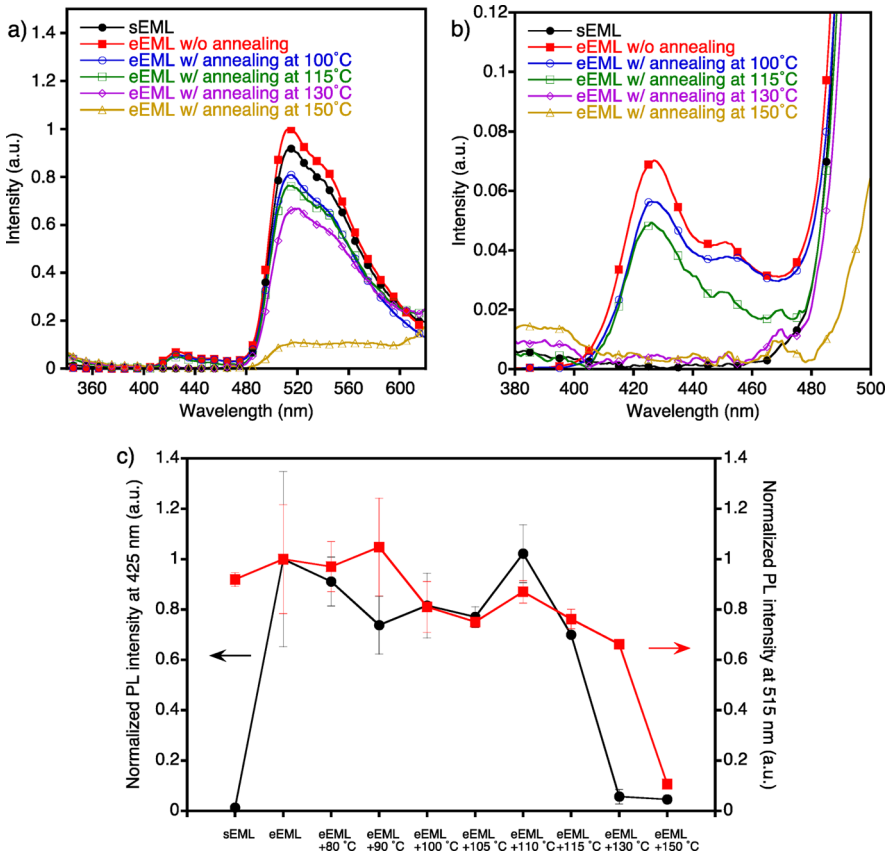

Figure 3. Results from fluorescence resonance energy transfer experiments. (a) Photoluminescence spectra of (●) PTPD/sEML; (■) PTPD/eEML without annealing; and PTPD/eEML with annealing at (○) 100, (□) 115, (◊) 130, and (△) 150 °C. (b) Expanded spectra in 380−500 nm region. (c) Normalized photoluminescence intensities of the films at 425 nm emission derived from PTPD and 515 nm emission derived from $Ir(mppy)_3$. eEML, evaporated BCzBP-d_{14}:9 wt % $Ir(mppy)_3$; and sEML, spin-coated BCzBP-d_{14}:9 wt % $Ir(mppy)_3$. Each spectra was normalized to the PL intensity of [PTPD/eEML w/o annealing]. Each error bar represents maximum and minimum values of three measurements.

was spin coated as sEML or evaporated as eEML on the PTPD layer. The [PTPD/sEML] and [PTPD/eEML] was not thermal annealed. Figure 3 shows photoluminescence spectra and plots of the photoluminescence intensities at 425 nm emission derived from PTPD and 515 nm emission derived from $Ir(mppy)_3$. In [PTPD/eEML] films, emissions derived from PTPD and $Ir(mppy)_3$ were observed. In contrast, in the [PTPD/sEML] film, fluorescence of PTPD was not observed. This indicates that the sEML molecules diffused into the PTPD layer during the solution process and fluorescence was quenched by $Ir(mppy)_3$ through the energy transfer mechanism.[26,27] This is supported by sufficient spectral overlaps between the absorption of the $Ir(mppy)_3$ film and the photoluminescence of the PTPD film (Figure S10).

We evaluated thermal diffusion in the stacked films by FRET to support the NR results by the FRET results. However, as previously indicated, the [PTPD/sEML without annealing] film showed no fluorescence of PTPD. On the other hand, the [PTPD/eEML] film showed fluorescence of PTPD, which enabled the analyses of the thermal diffusion. Of course, there is a differnce in the diffusion behaviors between the solution- and evaporation-process stacked films. However, we believe that the results of [PTPD/annealed-eEML] support the NR results. BCzBP:$Ir(mppy)_3$ layers were formed on PTPD by the evaporation process (eEML). These stacked films were thermal annealed at the several temperatures ranging from 80 to 150 °C for 10 min. Emission intensity of PTPD rapidly decreased after the annealing at 130 °C, indicating that the small molecules of eEML thermal diffused into PTPD at temperatures above T_g of the small molecules, and energy transfer from PTPD to $Ir(mppy)_3$ occurred. Although slight PL intensities of the films annealed at temperatures over 130 °C were plotted in Figure 3c, they are within noise levels. In contrast, the emission intensity of $Ir(mppy)_3$ remained high after annealing at 130 °C, but it decreased after annealing at 150 °C. PTPD has a smaller lowest triplet energy (2.3 eV) than $Ir(mppy)_3$ (2.4 eV). Therefore, when PTPD diffuses into eEML, the phosphorescence emission of $Ir(mppy)_3$ can be quenched by PTPD through the Dexter mechanism.[27] These results also provide evidence for asymmetrical interdiffusion of the polymer and the small molecules, which is consistent with the results obtained from NR. Even at 100−130 °C, the annealing caused partially quenching of eEML. To investigate the influence of the thermal annealing process itself to the PL of eEML, the eEML film alone was annealed at 115, 130, and 150 °C. The thermal annealing suppressed the emission intensities from $Ir(mppy)_3$ (Figure S11), probably due to concentration quenching by aggregation of $Ir(mppy)_3$. Photoluminescence spectra of the PTPD single layer were also measured. PTPD was spin coated and annealed at 135 °C for 10 min. After annealing, the films were further thermal annealed at the temperatures ranging from 80 to 150 °C for 10 min. These films showed similar photoluminescence intensities (Figure S12). Therefore, the annealing-induced quenching of PTPD in [PTPD/eEML] is not ascribed to annealing-induced morphology change of PTPD film itself.

DOI: 10.1021/acsami.5b05818
ACS Appl. Mater. Interfaces 2015, 7, 20779−20785

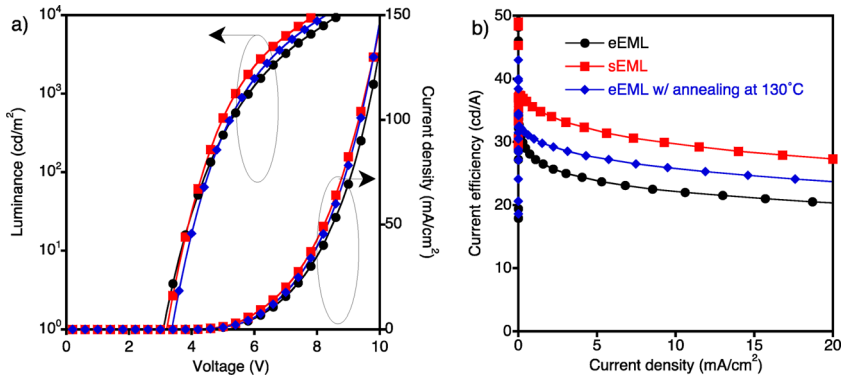

Figure 4. OLED characteristics. (a) Current density−voltage and luminance−voltage (JVL) characteristics and (b) current density−current efficiency characteristics of OLEDs with (●) eEML/eTPBi (device A), (■) sEML/eTPBi (device B), and (♦) eEML (annealed at 130 °C)/eTPBi (device C). eEML, evaporated BCzBP-d_{14}:9 wt % Ir(mppy)$_3$; sEML, spin-coated BCzBP-d_{14}:9 wt % Ir(mppy)$_3$.

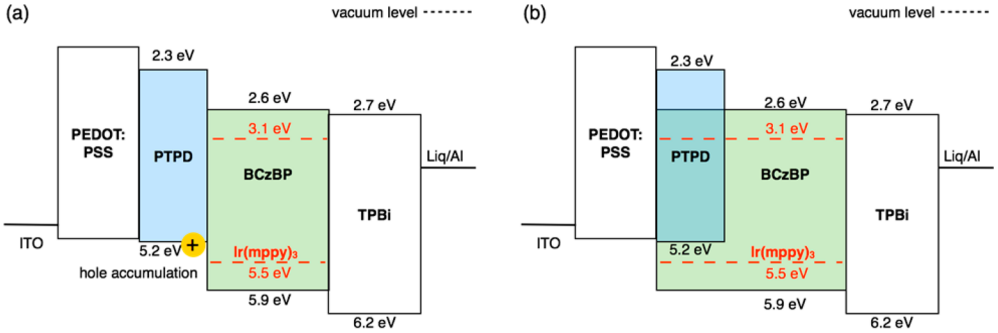

Figure 5. Description of multilayer structures and hole accumulation. Layer structure (a) without and (b) with layer mixing between PTPD and EML.

In cases of P3HT/PCBM bilayer films, it is well-known that degrees of crystallization of the materials influences diffusion behaviors.[12,15,16] P3HT and PCBM are materials to crystallize easily. In this study, we did not clearly observe crystallization in all films in a visual sense. Unlike the case of P3HT and PCBM, crystallizations of PTPD has not been discussed because, in the common fabrication process, applied temperatures do not exceed even the T_g of 224 °C. We also did not anneal the PTPD films at temperatures over the T_g. However, we observed changes of the PL intensity of PTPD, when the films were annealed at different temperatures for 10 min after spin-coatings (Figure S13). These changes suggest a possibility of film quality changes. On the other hand, BCzBP itself is likely to crystallize, but the addition of Ir(mppy)$_3$ inhibits the crystallization. The single-layer film did not show any changes by annealing at 150 °C in a visual sense. However, as previously mentioned, there is a possibility of aggregation of Ir(mppy)$_3$. The detailed analyses of the film quality changes of PTPD and EML, and effects of the changes on the mixing should be discussed in future works.

We fabricated OLEDs with structures of [ITO (130 nm)/poly(3,4-ethylenedioxythiophene):poly(4-styrenesulfonate) (PEDOT:PSS) (40 nm)/PTPD (20 nm)/BCzBP:9 wt % Ir(mppy)$_3$ (40 nm) as sEML or eEML/1,3,5-Tris(1-phenyl-1H-benzimidazol-2-yl)benzene (TPBi) (30 nm)/ 8-quinolinolato lithium (Liq) (1.5 nm)/Al (100 nm)]. The eEML was either not annealed or annealed at 130 °C for 10 min to diffuse the EML to the PTPD layer.

Device A: ITO/PEDOT:PSS/PTPD/eEML/eTPBi/Liq/Al

Device B: ITO/PEDOT:PSS/PTPD/sEML (115 °C)/eTPBi/Liq/Al

Device C: ITO/PEDOT:PSS/PTPD/eEML (130 °C)/eTPBi/Liq/Al

Current density−voltage, luminance−voltage, and current density−current efficiency characteristics are shown in Figure 4 (and Figure S14). Devices A, B, and C showed almost the same current density−voltage characteristics regardless of the interfacial structure of [PTPD/EML], which would affect hole injection. This indicates that conduction of the device is largely determined by electron current. On the other hand, devices B and C showed higher efficiencies than that of device A. Although the eEML film annealed at 130 °C had lower PL efficiency than the eEML without annealing film (Figure S11), the current efficiency of device C is larger than that of device A. These are presumably due to less triplet-polaron quenching by less accumulated holes in the diffused interface between PTPD and EML. The effects of the interfaces on the hole accumulation were described in Figure 5. The layer mixing gave more chances to pass holes from PTPD to Ir(mppy)$_3$, suppressing the hole accumulation. The layer comprinsing of only EML molecules also remained because of asymmetric diffusion. The existence of the layer is a key to achieve the improved performances, because PTPD quenches the emission of Ir(mppy)$_3$. The efficiency of device B with sEML was higher than that of devices C with eEML. The reason is now under survey. In addition to the interfacial condition, the EML film quality may affect the current efficiency. The efficiencies were mainly influenced by the interface of PTPD and EML, suggesting that the charge recombination zone in EML was located close to PTPD. This is consistent with the electron-dominant current density−voltage characteristics.

DOI: 10.1021/acsami.5b05818
ACS Appl. Mater. Interfaces 2015, 7, 20779−20785

3. CONCLUSION

We precisely evaluated the interface structures of the solution processed bilayer consisting of the hole transporting polymer underlayer and the small molecule emitting upperlayer and interdiffusion between the layers by thermal annealing process, using NR and FRET measurement. The polymer was much harder to diffuse than the small molecules during the formation of the interface and under the thermal annealing. We elucidated the effect of the interfacial structure on OLED characteristics. Partially mixing interfaces improved the current efficiencies due to suppressed triplet-polaron quenching in the interface. Controlling and understanding the interfacial structure of the miultilayers will be more important to improve the OLED characteristics.

4. EXPERIMENTAL SECTION

4.1. Materials and Film Preparation. Materials except for BCzBP and BCzBP-d_{14} were purchased from commercial sources. BCzBP was synthesized according to established procedures.[28] Deuterated BCzBP-d_{14} was synthesized as described in the Supporting Information. BCzBP, BCzBP-d_{14}, Ir(mppy)$_3$, and TPBi were purified by sublimation. Other materials were used as received. The substrates were rinsed with acetone and 2-propanol and then dried under a stream of clean nitrogen. Prior to film formation, the substrates were cleaned with a UV-ozone cleaner for 20 min. Films were formed by spin coating or evaporation under high vacuum ($<5.0 \times 10^{-5}$ Pa). Spin-coated PTPD and BCzBP:Ir(mppy)$_3$ (91:9 w/w) were formed from chlorobenzene and ester. Those films were annealed in a N_2-purged insulating container. PEDOT:PSS dispersion liquid was spin coated and annealed at 200 °C for 10 min in air. Thicknesses were determined using the results from neutron reflectometry or from a surface profilometer (Veeco Dektak8).

4.2. Neutron Reflectometry. Precleaned cut silicon (Si) wafers (KST World Corp., Japan) of 45 × 45 mm area were used without removal of the native oxide layer. Films were sequentially deposited by spin coating or evaporation onto the Si wafers. Neutron reflectivity were recorded using the single-frame mode of a SOFIA (SOFt Interface Analyzer) horizontal-type time-of-flight neutron reflectometer ($2.0\ \text{Å} < \lambda < 8.8\ \text{Å}$) at J-PARC (Japan Proton Accelerator Research Complex)/MLF (Materials and Life Science Experimental Facility).[29,30] Neutron pulses were recorded on a two-dimensional scintillation counter, which consists of an A R3239 photomultiplier tube (Hamamatsu Photonics K. K., Hamamatsu, Japan) with a ZnS/^{6}LiF scintillator (Ohyo Koken, Fussa, Japan). Reflected beam spectra were collected at 0.30, 0.75, and 1.80°. Individual data points were combined. Direct beam measurements were collected under the same collimation condition as 0.30° and the same time-of-flight profile for the other angles was used. Least-squares analyses of the reflectivity profiles were performed using the Motofit reflectometry analysis program; interfacial roughness was included via a Nevot−Croce factor.[20,31,32]

4.3. Fluorescence Resonance Energy Transfer (FRET). Precleaned quartz substrates were used as the substrates. Stacked films with structures of [quartz/PTPD (20 nm)/BCzBP:9 wt % Ir(mppy)$_3$ (40 nm)] were fabricated. Each layer was sequentially deposited by evaporation or spin coating. Deposited films were encapsulated in glass caps with UV-cured resins and oxygen getters. Photoluminescence spectra were obtained using HORIBA JOBIN YVON Fluoromax-4. Illuminated areas of excitation light were defined using a mask. The influence of guided light was possibly decreased by paste black tape on the samples.

4.4. OLED Fabrication and Measurements. OLEDs were fabricated on precleaned ITO substrates (Asahi Glass Co., Ltd.). OLEDs with the structure of [ITO (130 nm)/PEDOT:PSS (40 nm)/PTPD (20 nm)/BCzBP:9 wt % Ir(mppy)$_3$ (40 nm)/TPBi (30 nm)/Liq (1.5 nm)/Al (100 nm)] were fabricated. Here, PEDOT:PSS and PTPD were spin-coated. BCzBP:9 wt % Ir(mppy)$_3$ was spin coated on PTPD as sEML and annealed at 115 °C for 10 min. BCzBP:9 wt % Ir(mppy)$_3$ was also evaporated on PTPD as eEML. The eEML was either not annealed or annealed at 130 °C for 10 min. TPBi, Liq, and Al were evaporated successively. Fabricated devices were encapsulated in glass caps with UV-cured resins and oxygen getters. The sizes of all emission areas were 2 mm × 2 mm. The current density−voltage characteristics and luminance−voltage characteristics of the OLEDs were measured using a current source Keithley 2400 and a luminance meter Konica Minolta CS-200, respectively. EL spectra were measured using a spectral radiance meter Konica Minolta CS-2000. Quantum efficiencies were calculated using the Lambertian assumption.

■ ASSOCIATED CONTENT

Supporting Information

The Supporting Information is available free of charge on the ACS Publications website at DOI: 10.1021/acsami.5b05818.

Absorption spectra, photoluminescence spectra, neutron reflectometry results, device characteristics, synthetic procedures, DSC results, ^{1}H and ^{13}C NMR spectra and mass spectra(PDF)

■ AUTHOR INFORMATION

Corresponding Authors

*E-mail: pu@yz.yamagata-u.ac.jp.

*E-mail: kid@yz.yamagata-u.ac.jp. Tel. & Fax: +81-238-26-3595.

Notes

The authors declare no competing financial interest.

■ ACKNOWLEDGMENTS

We would like to thank Sho Kagami for DSC measurements. We would like to thank the Strategic Promotion of Innovative R&D Program of Japan Science and Technology Agency (JST) for financial support. The NR experiment was approved by the Neutron Science Proposal Review Committee of J-PARC/MLF (Proposal No. 2014A0304) and supported by the Inter-University Research Program on Neutron Scattering of IMSS, KEK. Y.-J.P. thanks the PRESTO (Sakigake), JST for support.

■ REFERENCES

(1) Hagen, D. A.; Foster, B.; Stevens, B.; Grunlan, J. C. Shift-Time Polyelectrolyte Multi layer Assembly: Fast Film Growth and High Gas Barrier with Fewer Layers by Adjusting Deposition Time. *ACS Macro Lett.* **2014**, *3*, 663−666.

(2) Lee, W.; Yoon, J.; Thomas, E. L.; Lee, H. Dynamic Changes in Structural Color of a Lamellar Block Copolymer Photonic Gel during Solvent Evaporation. *Macromolecules* **2013**, *46*, 6528−6532.

(3) Macleod, H. A. *Thin-film Optical Filters*; 4th ed.; CRC Press/Taylor & Francis: Boca Raton, FL, 2010.

(4) Sakai, H.; Umemura, J. Effect of Infrared Radiation and Air Flow on Fourier Transform Infrared External Reflection Spectra of Langmuir Monolayers. *Langmuir* **1997**, *13*, 502−505.

(5) Smith, A. R. G.; Lee, K. H.; Nelson, A.; James, M.; Burn, P. L.; Gentle, I. R. Diffusion - The Hidden Menace in Organic Optoelectronic Devices. *Adv. Mater.* **2012**, *24*, 822−826.

(6) Ohisa, S.; Matsuba, G.; Yamada, N. L.; Pu, Y.-J.; Sasabe, H.; Kido, J. Precise Evaluation of Angstrom-Ordered Mixed Interfaces in Solution-Processed OLEDs by Neutron Reflectometry. *Adv. Mater. Interfaces* **2014**, *1*, 1400097.

(7) Aizawa, N.; Pu, Y.-J.; Watanabe, M.; Chiba, T.; Ideta, K.; Toyota, N.; Igarashi, M.; Suzuri, Y.; Sasabe, H.; Kido, J. Solution-Processed Multilayer Small-molecule Light-emitting Devices with High-efficiency White-light Emission. *Nat. Commun.* **2014**, *5*, 5756.

(8) Zhou, Y. H.; Fuentes-Hernandez, C.; Shim, J.; Meyer, J.; Giordano, A. J.; Li, H.; Winget, P.; Papadopoulos, T.; Cheun, H.; Kim, J.; Fenoll, M.; Dindar, A.; Haske, W.; Najafabadi, E.; Khan, T. M.;

DOI: 10.1021/acsami.5b05818
ACS Appl. Mater. Interfaces 2015, 7, 20779−20785

Sojoudi, H.; Barlow, S.; Graham, S.; Bredas, J. L.; Marder, S. R.; Kahn, A.; Kippelen, B. A Universal Method to Produce Low-Work Function Electrodes for Organic Electronics. *Science* **2012**, *336*, 327−332.
(9) Jasieniak, J. J.; Seifter, J.; Jo, J.; Mates, T.; Heeger, A. J. A Solution-Processed MoOx Anode Interlayer for Use within Organic Photovoltaic Devices. *Adv. Funct. Mater.* **2012**, *22*, 2594−2605.
(10) Chiba, T.; Pu, Y.-J.; Hirasawa, M.; Masuhara, A.; Sasabe, H.; Kido, J. Solution-Processed Inorganic-Organic Hybrid Electron Injection Layer for Polymer Light-Emitting Devices. *ACS Appl. Mater. Interfaces* **2012**, *4*, 6104−6108.
(11) Earmme, T.; Ahmed, E.; Jenekhe, S. A. Solution-Processed Highly Efficient Blue Phosphorescent Polymer Light-Emitting Diodes Enabled by a New Electron Transport Material. *Adv. Mater.* **2010**, *22*, 4744−4748.
(12) Môn, D.; Higgins, A. M.; James, D.; Hampton, M.; Macdonald, J. E.; Ward, M. B.; Gutfreund, P.; Lilliu, S.; Rawle, J. Bimodal Crystallization at Polymer-Fullerene Interfaces. *Phys. Chem. Chem. Phys.* **2015**, *17*, 2216−2227.
(13) Clulow, A. J.; Tao, C.; Lee, K. H.; Velusamy, M.; McEwan, J. A.; Shaw, P. E.; Yamada, N. L.; James, M.; Burn, P. L.; Gentle, I. R.; Meredith, P. Time-Resolved Neutron Reflectometry and Photovoltaic Device Studies on Sequentially Deposited PCDTBT-Fullerene Layers. *Langmuir* **2014**, *30*, 11474−11484.
(14) Tao, C.; Aljada, M.; Shaw, P. E.; Lee, K. H.; Cavaye, H.; Balfour, M. N.; Borthwick, R. J.; James, M.; Burn, P. L.; Gentle, I. R.; Meredith, P. Controlling Hierarchy in Solution-processed Polymer Solar Cells Based on Crosslinked P3HT. *Adv. Energy Mater.* **2013**, *3*, 105−112.
(15) Ro, H. W.; Akgun, B.; O'Connor, B. T.; Hammond, M.; Kline, R. J.; Snyder, C. R.; Satija, S. K.; Ayzner, A. L.; Toney, M. F.; Soles, C. L.; DeLongchamp, D. M. Poly(3-hexylthiophene) and [6,6]-Phenyl-C-61-butyric Acid Methyl Ester Mixing in Organic Solar Cells. *Macromolecules* **2012**, *45*, 6587−6599.
(16) Chen, D.; Liu, F.; Wang, C.; Nakahara, A.; Russell, T. P. Bulk Heterojunction Photovoltaic Active Layers via Bilayer Interdiffusion. *Nano Lett.* **2011**, *11*, 2071−2078.
(17) Higgins, A. M.; Cadby, A.; Lidzey, D. G.; Dalgliesh, R. M.; Geoghegan, M.; Jones, R. A. L.; Martin, S. J.; Heriot, S. Y. The impact of Interfacial Mixing on Forster Transfer at Conjugated Polymer Heterojunctions. *Adv. Funct. Mater.* **2009**, *19*, 157−163.
(18) Higgins, A. M.; Martin, S. J.; Geoghegan, M.; Heriot, S. Y.; Thompson, R. L.; Cubitt, R.; Dalgliesh, R. M.; Grizzi, I.; Jones, R. A. L. Interfacial Structure in Conjugated Polymers: Characterization and Control of the Interface between Poly(9,9-dioctylfluorene) and Poly(9,9-dioctylfluorene-alt-benzothiadiazole). *Macromolecules* **2006**, *39*, 6699−6707.
(19) Roe, R. J. *Methods of X-ray and Neutron Scattering in Polymer Science*; Oxford University Press: New York, 2000.
(20) Nevot, L.; Croce, P. Caractérisation des Surfaces par Réflexion Rasante de Rayons X. Application à L'étude du Polissage de Quelques Verres Silicates. *Rev. Phys. Appl.* **1980**, *15*, 761−779.
(21) Parratt, L. G. Surface Studies of Solids by Total Reflection of X-Rays. *Phys. Rev.* **1954**, *95*, 359−369.
(22) Komino, T.; Nomura, H.; Yahiro, M.; Adachi, C. Reorganization of the Molecular Orientation at the Organic/Substrate Interface in Spirofluorene Thin Films. *Chem. Phys. Lett.* **2013**, *563*, 70−75.
(23) Komino, T.; Nomura, H.; Yahiro, M.; Adachi, C. Real-Time Measurement of Molecular Orientational Randomization Dynamics during Annealing Treatments by In-Situ Ellipsometry. *J. Phys. Chem. C* **2012**, *116*, 11584−11588.
(24) Inoue, R.; Kawashima, K.; Matsui, K.; Kanaya, T.; Nishida, K.; Matsuba, G.; Hino, M. Distributions of Glass-transition Temperature and Thermal Expansivity in Multilayered Polystyrene Thin Films Studied by Neutron Reflectivity. *Phys. Rev. E* **2011**, *83*, 021801.
(25) Campoy-Quiles, M.; Sims, M.; Etchegoin, P. G.; Bradley, D. D. C. Thickness-dependent Thermal Transition Temperatures in Thin Conjugated Polymer Films. *Macromolecules* **2006**, *39*, 7673−7680.
(26) Förster, T. 10th Spiers Memorial Lecture. Transfer Mechanisms of Electronic Excitation. *Discuss. Faraday Soc.* **1959**, *27*, 7−17.
(27) Dexter, D. L. A Theory of Sensitized Luminescence in Solids. *J. Chem. Phys.* **1953**, *21*, 836−850.
(28) Jun, C. H.; Pu, Y.-J.; Igarashi, M.; Chiba, T.; Sasabe, H.; Kido, J. A Donor-Acceptor-type Host Material for Solution-processed Phosphorescent Organic Light-emitting Devices Showing High Efficiency. *Chem. Lett.* **2014**, *43*, 1935−1936.
(29) Mitamura, K.; Yamada, N. L.; Sagehashi, H.; Torikai, N.; Arita, H.; Terada, M.; Kobayashi, M.; Sato, S.; Seto, H.; Goko, S.; Furusaka, M.; Oda, T.; Hino, M.; Jinnai, H.; Takahara, A. Novel Neutron Reflectometer SOFIA at J-PARC/MLF for In-situ Soft-interface Characterization. *Polym. J.* **2013**, *45*, 100−108.
(30) Yamada, N. L.; Torikai, N.; Mitamura, K.; Sagehashi, H.; Sato, S.; Seto, H.; Sugita, T.; Goko, S.; Furusaka, M.; Oda, T.; Hino, M.; Fujiwara, T.; Takahashi, H.; Takahara, A. Design and Performance of Horizontal-type Neutron Reflectometer SOFIA at J-PARC/MLF. *Eur. Phys. J. Plus* **2011**, *126*, 108.
(31) Nelson, A. Motofit−integrating Neutron Reflectometry Acquisition, Reduction and Analysis into One, Easy to Use, Package. *J. Phys.: Conf. Ser.* **2010**, *251*, 012094.
(32) Nelson, A. Co-refinement of Multiple-contrast Neutron/X-ray Reflectivity Data Using MOTOFIT. *J. Appl. Crystallogr.* **2006**, *39*, 273−276.

DOI: 10.1021/acsami.5b05818
ACS Appl. Mater. Interfaces 2015, 7, 20779−20785